Journal of Alloys and Compounds 509 (2011) 8549–8553

Contents lists available at ScienceDirect

Journal of Alloys and Compounds

journal homepage: www.elsevier.com/locate/jallcom

Size-controlled synthesis of monodisperse superparamagnetic iron oxide nanoparticles

Yuan Zhu[a,b], F.Y. Jiang[b,c], Kexin Chen[a,*], Feiyu Kang[a], Z.K. Tang[b,**]

[a] Department of Materials Science and Engineering, Tsinghua University, Beijing, China
[b] Department of Physics, The Hong Kong University of Science and Technology, Clear Water Bay, Hong Kong, China
[c] School of Environment and Materials Engineering, Yantai University, Qingquan Road, Laishan Zone, Yantai, China

ARTICLE INFO

Article history:
Received 4 March 2011
Received in revised form 29 May 2011
Accepted 31 May 2011
Available online 17 June 2011

Keywords:
Magnetic materials
Nanomaterials
Thermal decomposition

ABSTRACT

Monodisperse iron oxide nanoparticles were prepared by thermal decomposition of iron carbonyl in octyl ether in the presence of oleic acid. The particle size could be tuned from 7 nm to 25 nm. The dual role of oleic acid as a surfactant and a boiling-point elevating agent was discussed. The impacts of varied reflux conditions were investigated and a new monodisperse mechanism was given. High-resolution transmission electron microscopy (HRTEM) and selected area electron diffraction (SAED) were used to study the oxidation states of iron oxide nanoparticles. The evolution of *d*-spacing values in HRTEM images and SAED patterns demonstrated the transition from γ-Fe_2O_3 to Fe_3O_4 with the increasing particle size. Superconducting quantum interference device (SQUID) and vibrating sample magnetometer (VSM) were used to reveal the superparamagnetic behavior of as-synthesized nanoparticles.

1. Introduction

The synthesis of magnetic nanoparticles has attracted renewed research interest in recent years, driven by their new applications such as advanced magnetic materials [1–5], ultra high-density magnetic storage media [6] and biological imaging [7]. Among these magnetic nanoparticles, iron oxides (Fe_2O_3 and Fe_3O_4) have been extensively investigated due to its excellent performance. Their unique properties crucially depend on their size and size distribution.Various routes to synthesize iron oxide nanoparticles have been developed, such as coprecipitation [8], hydrolysis of iron salt [9], decomposition of organic iron precursor [10–12], hydrothermal and solvothermal methods [13,14]. Thermal decomposition of iron carbonyl is one of the most used methods. It was first developed in the late 1970s using decalin (cis- and trans-decahydronaphthalene) as solvent [10,11], and then improved by a number of researchers with other solvents [15–22]. Hyeon et al. [15,16] used various solvents with different boiling points to demonstrate the dependence of particle size on aging temperature and time. Teng and Yang [22] noticed that different aging temperatures, namely reflux or pre-reflux temperatures, had different impacts on the resulting particle size and size distribution. In a typical octyl ether (solvent)/oleic acid (surfactant) system, we discover the dual role of oleic acid in encapsulating the nanoparticles and elevating the reflux temperature. With careful control of the oleic acid amount, we can tune the boiling point of the reaction mixture in a continuous interval, which is more flexible than using various solvents of discrete boiling points. The reflux states are found crucial in monodisperse mechanisms.

2. Experimental details

2.1. General

In a typical procedure, octyl ether and oleic acid were added into a three-necked flask under argon flow. After the mixture was heated right above 100 °C, iron pentacarbonyl was added into the flask with pipette. The resultant mixture was heated to reflux. After keeping refluxing for a given time, the mixture was smoothly cooled to 150 °C and oxidized for 1 h. The suspension was then cooled to room temperature and the nanoparticles were collected by ethanol wash and centrifuging. The collected iron oxide nanoparticles were well dispersed in cyclohexane.

2.2. Reflux procedures

The reflux procedures were carefully controlled. Different combinations of pre-reflux (when the temperature is kept 5–10 °C lower than boiling point) and vigorous reflux (boiling) were examined. A typical procedure was boiling for 20 min followed by pre-refluxing for several hours.

2.3. Oxidization procedures

The oxidation of the particles was conducted when the refluxed mixture was cool to 150 °C. A typical oxidation method was simply aeration for 1 h at this temperature. An alternative approach was adding oxidant $(CH)_3NO$ in argon atmosphere. Here $(CH)_3NO$ is reported to be a widely used mild oxidant for preparing γ-Fe_2O_3.

* Corresponding author. Tel.: +86 10 62772548; fax: +86 10 62772548.
** Corresponding author. Tel.: +852 23587972; fax: +852 23581652.
E-mail addresses: zhuyuan02@mails.thu.edu.cn (Y. Zhu), kxchen@mail.tsinghua.edu.cn (K. Chen), phzktang@ust.hk (Z.K. Tang).

0925-8388/$ – see front matter © 2011 Elsevier B.V. All rights reserved.
doi:10.1016/j.jallcom.2011.05.115

Table 1
List of compositions of the investigated reaction system, aging time, and resulting particle sizes.

#	Octyl ether (mL)	$Fe(CO)_5$ (mmol)	Oleic acid (mmol)	Molar ratio of oleic acid to ($Fe(CO)_5$), *R*	Concentration of oleic acid (mmol/mL)	Pre-reflux time (h)	Resulting particle size (nm)
1	10	1.84	7	3.8	0.7	2	7
2	10	1.84	7	3.8	0.7	4	10
3	10	3.07	12.25	4.0	1.23	1.5	15
4	9	2.3	10.5	4.6	1.17	3	22

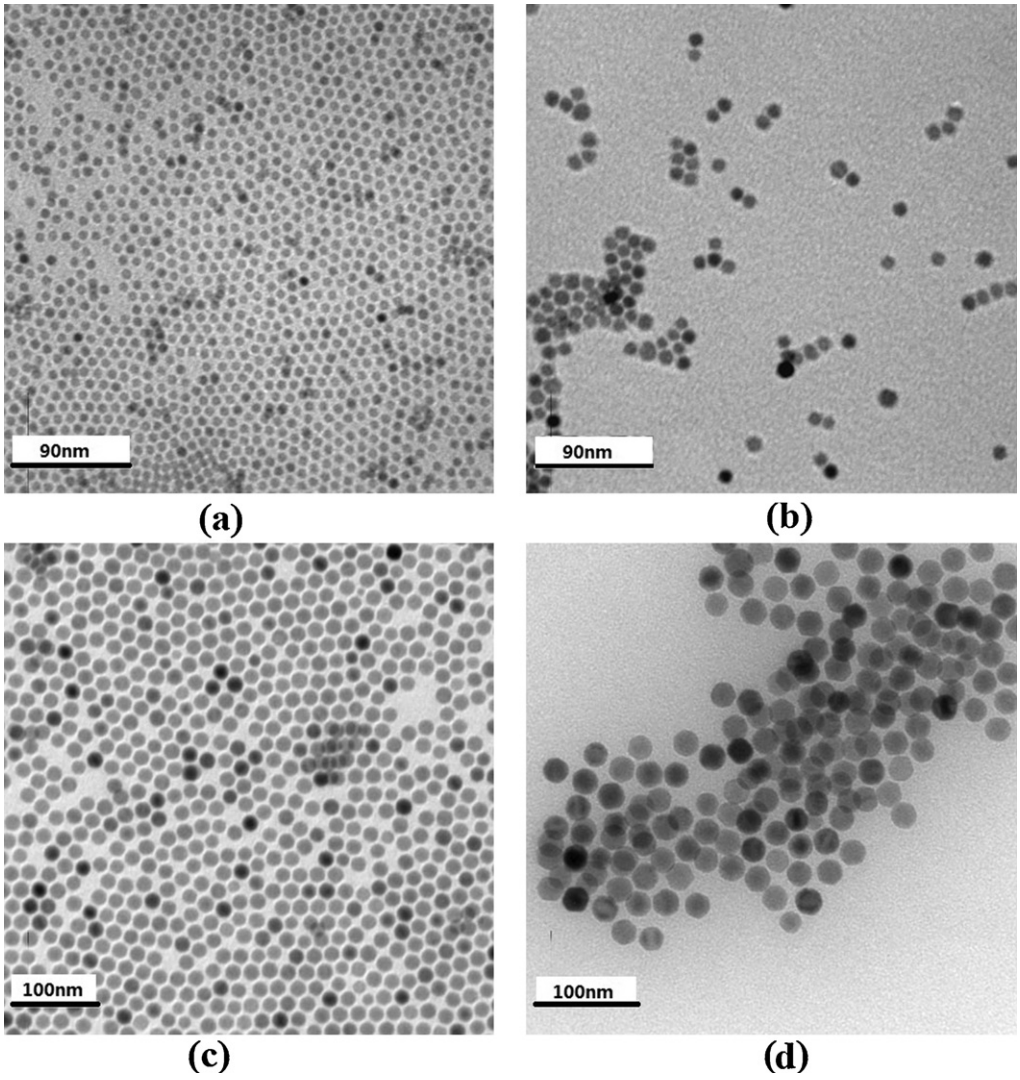

Fig. 1. TEM images of monodisperse iron oxide nanocrystals: (a) 7 nm; (b) 10 nm; (c) 15 nm; (d) 22 nm.

2.4. Characterizations

Nanoparticles were characterized by low- and high-resolution transmission electron microscopy (HRTEM) and selected area electron diffraction (SAED). The magnetic properties were studied by superconducting quantum interference device (SQUID) and vibrating sample magnetometer (VSM).

3. Results and discussion

3.1. Dual role of oleic acid

Using general synthesis method with typical reflux and oxidation procedures, particle size could be tuned from 7 to 22 nm under different reaction conditions (detailed in Table 1). All the resulting nanoparticles were of high uniformity (Fig. 1). The particle size increases with the molar ratio, *R*, of oleic acid to $Fe(CO)_5$. Given the same *R*, the particle size also increases with the reflux time. These results accord well with Hyoen's and Teng's works.

The positive correlation between the particle size and *R*, however, does not stand much physical sense if we take oleic acid only as a surfactant. Being a surfactant, the oleic acid's usage should be lowered since surface area decreases when the same amount of iron oxides form larger particles. Thus oleic acid may play a role other than surfactant. According to Raoult's law, the elevation of boiling point (bp) of the solution can be attributed to the adding of the less volatile solute. Here oleic acid (bp 360 °C) is less volatile than octyl ether (bp 289 °C) and can readily functionalize as a boiling-point elevating agent in the reaction system. Higher oleic acid concentration, *C*, suggests higher boiling point. It was revealed that particle size increased in response to the increase in the reflux temperature

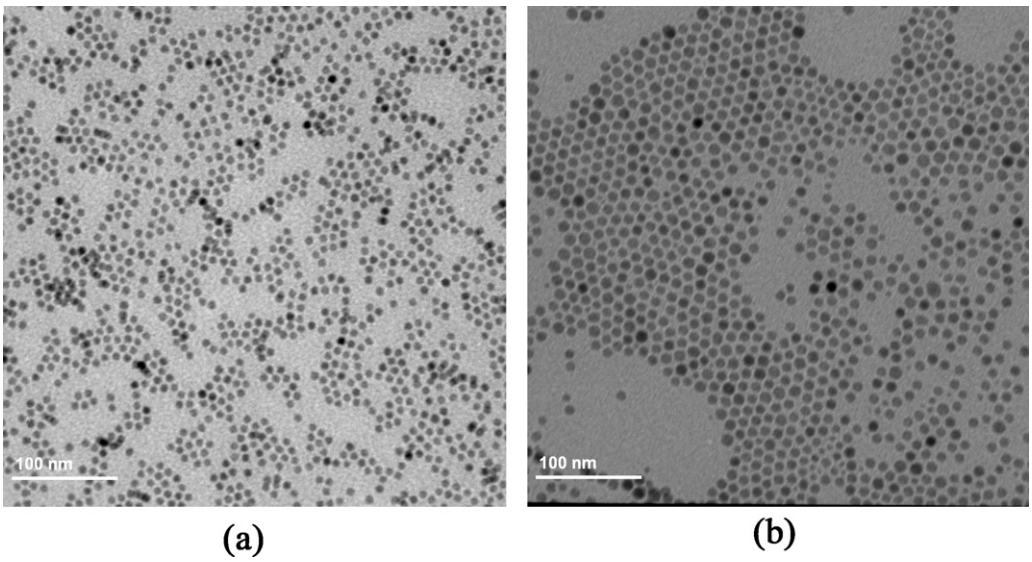

Fig. 2. (a) TEM images of resulting particles from reference experiment; (b) TEM images of resulting particles from contrast experiment.

[15]. From above two points, we can deduce that higher *C* leads to bigger resultant particle size. The positive correlation between resultant particle size and *C* is more self-explanatory than that between particle size and *R*.

To justify our deduction, the influence of the oleic acid concentration should be investigated more specifically. We took the 1# reaction system in Table 1 as a reference and designed a contrast experiment. In designed experiment, *C* was increased from 0.7 mmol/mL to 1.05 mmol/mL. To exclude the perturbations of *R* and reflux time, their values were lowered to 3.5 and 1.3 h, respectively. In the well designed contrast experiment, the boiling point of the mixture rose to ~320 °C while that of the reference reaction was only ~310 °C. The increase of *C* was sufficient to elevate the boiling point. The TEM images of resulting particles are shown in Fig. 2. The particle size of the reference reaction is 7 nm (Fig. 2a) whereas that of the contrast experiment is 11 nm (Fig. 2b). Although the size distribution of 11 nm particles is somehow wider than that of 7 nm particles, the dependence of the particle size on *C* and thus the reflux temperature is clear. The widening of the size distribution may be owing to the shortened reflux time.

To summarize, oleic acid, first known as a surfactant in this reaction system, now is also found as a boiling-point elevating agent. By regulating the oleic acid concentration, the reflux temperature can be altered in a continuous interval. This is more facile and flexible than using various solvents with discrete boiling points.

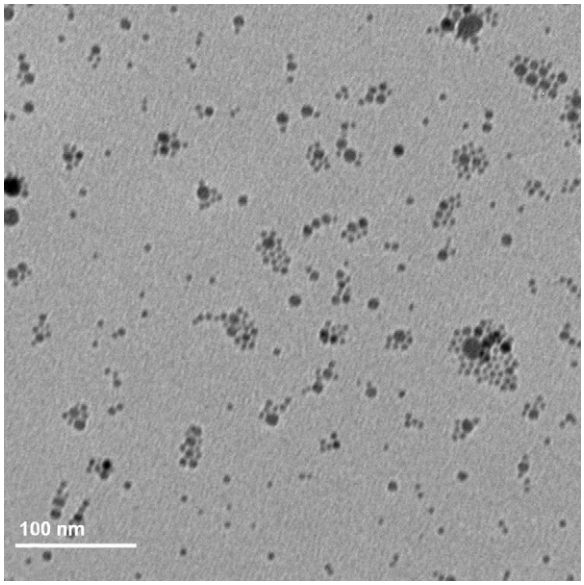

Fig. 3. TEM images of polydisperse particles from badly-designed reflux procedure (pre-reflux followed by vigorous reflux).

3.2. Monodisperse mechanisms

It is ascertained that the iron-oleate complexes, which are generated *in situ* from the reaction of $Fe(CO)_5$ and oleic acid, decompose and act effectively as precursors for iron oxide nanoparticles [16]. Their TGA/DSC patterns revealed that one oleate ligand disassociates from the precursor at 200–240 °C and the remaining two disassociate at 300 °C [16]. The space effect of the oleate ligands may impede the effective collision among iron-oleate complexes until the ligands begin to leave. The nucleation could start after the removal of impedient ligands. For monodisperse nanoparticles, a tedious Ostwald ripening process is inevitable.

In our work, however, a kinetic way was found useful to accelerate the nucleation and growth of the iron oxide nanoparticles. The key of speedup is to handle the reflux procedure very carefully. Different combinations of pre-reflux (5–10 °C lower than boiling point) and vigorous reflux (boiling) will render the kinetic energy of the reaction mixture varied. Vigorous reflux procedure with higher kinetic energy may enhance the nucleation by increasing particles' velocity and collision probability. When the reaction mixture was treated by vigorous reflux of 20 min and followed by pre-reflux of several hours, monodisperse particles were produced (Fig. 1). In another experiment, the reflux procedure was pre-refluxing of 3 h followed by vigorously boiling of 20 min. The uniformity of the collected particles is relatively poor (Fig. 3). It may be concluded that vigorous reflux is a nucleation favored procedure and pre-reflux is a growth favored procedure. When vigorously refluxed, iron-oleate complexes frequently collide with each other aided by turbulent flows and thus trigger the nucleation. In a following pre-reflux period, the residue iron-oleate complexes are more intended to grow on surface of the nucleated particles, driven by thermodynamics. The nucleation here is laid aside. As a result, the nucleation process and the growth process are separated successfully, which ensured the uniformity of the particles. Given the two reflux steps being switched, the later vigorous reflux

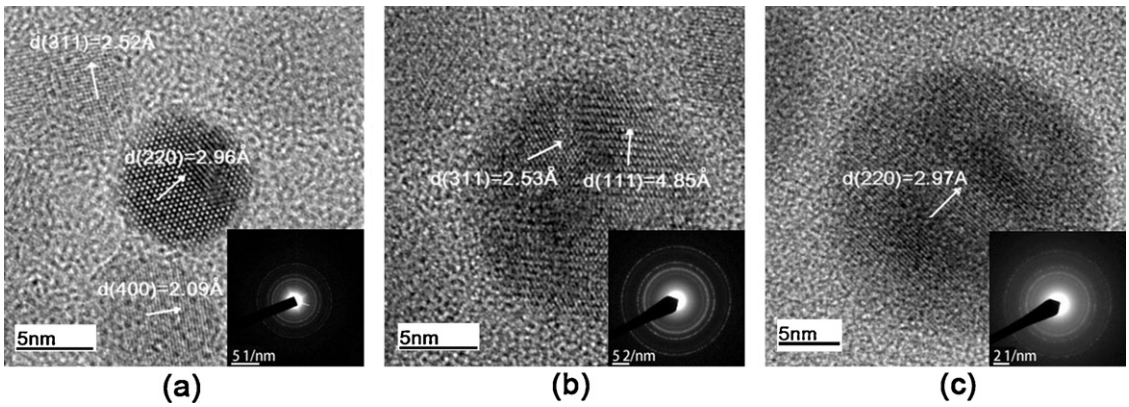

Fig. 4. HRTEM images and SAED patterns (inlet) of aeration-oxidized nanoparticles: (a) 7 nm; (b) 15 nm; (c) 22 nm.

Table 2
SAED *d*-spacing values (Å) of 7 nm, 15 nm, and 22 nm iron oxide particles in Fig. 4.

(*hlk*)	Resulting particle size			Standard γ-Fe_2O_3	Standard Fe_3O_4
	(7 nm)	(15 nm)	(22 nm)		
(1 1 1)				4.82	4.85
(2 2 0)	2.952		2.966	2.953	2.967
(3 1 1)	2.516	2.524	2.528	2.518	2.532
(4 0 0)	2.086	2.095	2.098	2.089	2.099
(5 1 1)	1.606	1.618	1.618	1.607	1.616
(4 4 0)	1.480	1.484	1.486	1.476	1.485

will lead to a second-time nucleation and thus polydisperse particles.

3.3. Oxidation states

The aeration method was used as a typical way of oxidization in all above experiments. To reveal the effects of aeration oxidation on the fine crystal structures and oxidation states (i.e. γ-Fe_2O_3 or Fe_3O_4) of the resultant iron oxide, 7 nm, 15 nm and 22 nm iron oxides in Fig. 1 were observed under HRTEM and SAED (Fig. 4). The (3 1 1) spacing value of 7 nm nanocrystal is 2.52 Å while that of 15 nm is 2.53 Å. This minor discrepancy readily implies that their dominant phases are different, since γ-Fe_2O_3 and Fe_3O_4 have almost the same spinel structure with only ~1% difference between their lattice constants. For comparison, each *d*-spacing value from SAED was calculated by graphics software (Digital Micrograph Demo) and listed in Table 2. By examining the *d*-spacing values of (2 2 0), (3 1 1), (4 0 0), (5 1 1), and (4 4 0) planes in each sample (except the invisible (2 2 0) planes of 15 nm particles), it is noted that γ-Fe_2O_3 is the dominant phase of small-sized iron oxide nanoparticles and the proportion of the Fe_3O_4 component gradually increases with the particle size.

An alternative oxidation method using $(CH)_3NO$ in argon atmosphere was compared with the aeration method. In aeration experiment, a portion of the reaction mixture before it was exposed to air flow was collected and kept in argon atmosphere. Sufficient amount of $(CH)_3NO$ (i.e. triple of the $Fe(CO)_5$ mole amount) was then added into the collected portion. The reaction could be smelly owing to the release of NH_3 as a byproduct. Iron oxide nanoparticles with size of 7 nm, 15 nm, and 25 nm were prepared. The HRTEM and SAED images of the resulting nanoparticles are shown in Fig. 5. The (4 0 0) spacing value of 7 nm nanocrystal is 2.09 Å, while that of 15 nm is 2.10 Å. The (1 1 1) spacing value of 25 nm nanocrystal is 4.85 Å. Compared with the standard JCPDS data of γ-Fe_2O_3 and Fe_3O_4 given in Table 2, these *d*-spacing values also imply the transition from γ-Fe_2O_3 to Fe_3O_4 with the increasing particle size. $(CH)_3NO$, though reported useful for preparing γ-Fe_2O_3 particles of 16 nm and 25 nm [22], was found not superior to aeration in oxidation capability.

3.4. Magnetic properties

Preliminary magnetic measurements were performed in the iron oxide nanoparticles using superconducting quantum interference device and vibrating sample magnetometer. The dependence of the magnetization on temperature was measured with the use of zero-field cooling procedures in an applied magnetic field of 100 Oe between 5 K and 300 K. The plots of magnetization versus temperature (Fig. 6) reveal the superparamagnetic behavior of 7 nm, 15 nm and 25 nm iron oxide nanoparticles at higher temperatures. The

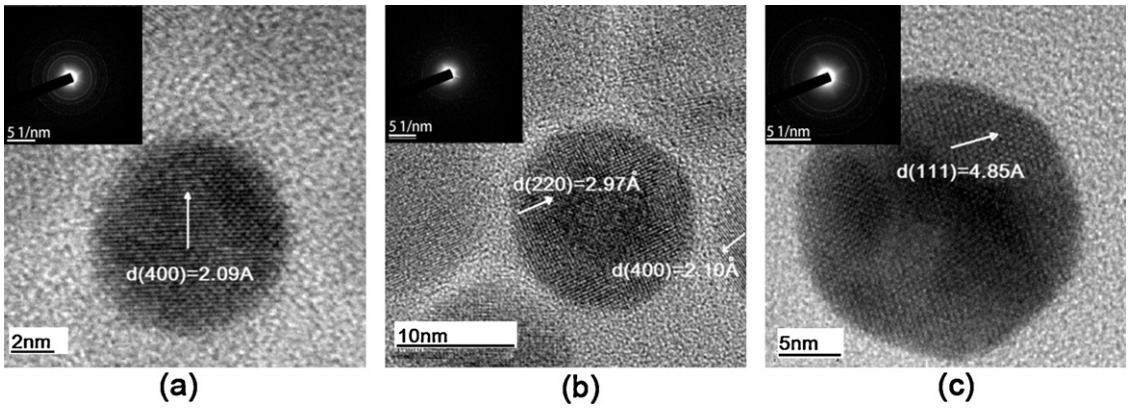

Fig. 5. HRTEM images and SAED patterns (inlet) of $(CH)_3NO$-oxidized nanoparticles: (a) 7 nm; (b) 15 nm; (c) 25 nm.

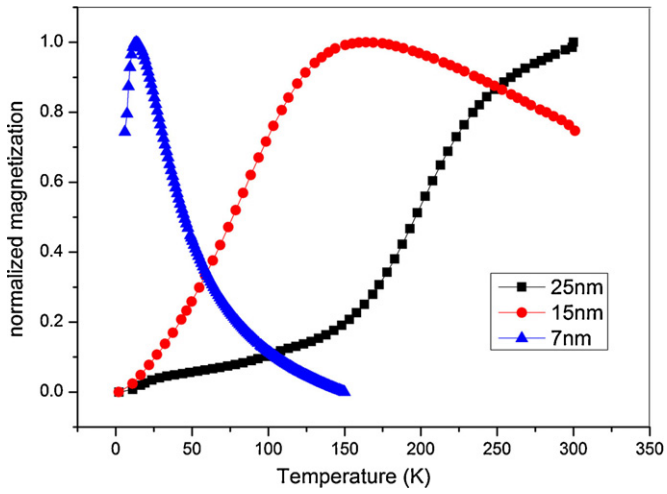

Fig. 6. Magnetization versus temperature for 7 nm (triangles), 15 nm (circles) and 25 nm (squares) iron oxide nanoparticles with zero-field cooling at the applied magnetic field of 100 Oe (SQUID results).

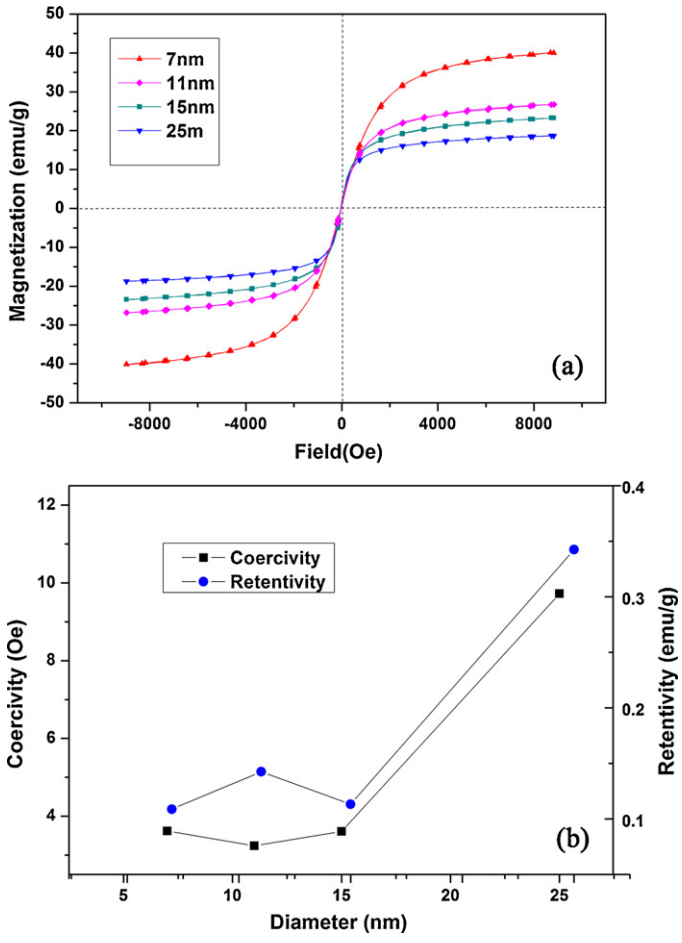

Fig. 7. (a) Room temperature magnetization curves of 7 nm (uptriangles), 11 nm (diamonds), 15 nm (squares) and 25 nm (downtriangles) iron oxide nanoparticles. (b) Retentivity and coercive force versus particle size (VSM results).

blocking temperatures (T_B) of 7 nm, 15 nm and 25 nm iron oxide nanoparticles are 14 K, 164 K, and more than 300 K, respectively.

Fig. 7a shows the magnetic hysteresis loops for the as-prepared iron oxide particles of 7 nm, 11 nm, 15 nm, 25 nm at 300 K. The nearly zero retentivity and coercivity suggest that all the samples are superparamagnetic at room temperature. More detailed plots of retentivity or coercivity versus particle size are presented in Fig. 7b. Both retentivity and coercivity undergo a steep rise around the particle size of 25 nm. It was calculated that the critical particle size of ferromagnetism of magnetite is ~25 nm at room temperature [23]. We can conclude the similar by the observation that T_B of 25 nm iron oxide was higher than 300 K. The as-prepared 25 nm iron oxide particles showed weak hysteresis at room temperature. Its absolute value of coercivity (~9 Oe) is far less than that of bulk magnetite but of the same order of magnitude with 7 nm, 11 nm, 15 nm iron oxide particles. So 25 nm iron oxide particles can approximately be taken as superparamagnetic at room temperature.

4. Conclusions

Monodisperse superparamagnetic iron oxide nanoparticles were fabricated from the controlled decomposition of iron pentacarbonyl ($Fe(CO)_5$) in octyl ether. The resulting particle size can be tuned from 7 nm to 25 nm by alternating the reaction mixture compositions and aging conditions. The oleic acid was found to play a dual role in the reaction system. It functionalizes not only as a surfactant but also as a boiling-point elevating agent. With its help, the boiling point of the reaction mixture could be elevated and leads to an increase in the resulting particle size. The size distributions of the as-prepared particles were very narrow, which could be attributed to the very carefully control of the reflux procedure. The particle size influences the oxidation states of the iron oxides (i.e. γ-Fe_2O_3 or Fe_3O_4). γ-Fe_2O_3 was the dominant phase of small-sized iron oxide nanocrystals, whereas the proportion of the Fe_3O_4 component gradually increased with the particle size. This result is not likely to be affected by the use of $(CH)_3NO$.

Acknowledgments

This work was supported by National High Technology Research and Development Program of China (2009AA03Z211), National Natural Science Foundation of China (50972123), Natural Science Foundation of Shandong Province, China (Y2007F19), and HKUST RPC 07/08.SC.05.

References

[1] H. Zeng, J. Li, J. Liu, Z. Wang, S. Sun, Nature 420 (2002) 395–398.
[2] T. Zhang, D. Zhao, L. Yin, Z. Shen, J. Alloys Compd. 508 (2010) 147–151.
[3] D. Sellmyer, Nature 420 (2002) 374–375.
[4] X. Teng, H. Yang, J. Am. Chem. Soc. 125 (2003) 14559–14563.
[5] M. Parra-Borderias, F. Bartolome, J. Herrero-Albillos, L. Garcia, J. Alloys Compd. 481 (2009) 48–56.
[6] S. Sun, C. Murray, D. Weller, L. Folks, A. Moser, Science 287 (2000) 1989–1992.
[7] H. Kim, Y. Ahn, H.S. Lee, J. Alloys Compd. 434–435 (2007) 633–637.
[8] R. Valenzuela, M.C. Fuentes, C. Parra, J. Baeza, N. Duran, S.K. Sharma, M. Knobel, J. Freer, J. Alloys Compd. 488 (2009) 227–231.
[9] T. Ozkaya, M. Toprak, A. Baykal, H. Kavas, Y. Koseoglu, B. Aktas, J. Alloys Compd. 472 (2009) 18–23.
[10] C.H. Griffiths, M.P. Ohoro, T.W. Smith, J. Appl. Phys. 50 (1979) 7108–7115.
[11] T.W. Smith, D. Wychick, J. Phys. Chem. 84 (1980) 1621–1629.
[12] R. Shi, X.H. Liu, G.H. Gao, R. Yi, Zh.G. Qiu, J. Alloys Compd. 485 (2009) 548–553.
[13] J. Chen, F.B. Wang, K.L. Huang, Y.N. Liu, S.Q. Liu, J. Alloys Compd. 475 (2009) 898–902.
[14] M. Srivastavaa, A.K. Ojhab, S. Chaubeya, J. Singhc, P.K. Sharmad, A.C. Pandeyd, J. Alloys Compd. 500 (2010) 206–210.
[15] T. Hyeon, S. Lee, J. Park, Y. Chung, H. Bin Na, J. Am. Chem. Soc. 123 (2001) 12798–12801.
[16] J. Park, K. An, Y. Hwang, J. Park, H. Noh, J. Kim, J. Park, N. Hwang, T. Hyeon, Nat. Mater. 3 (2004) 891–895.
[17] N. Feltin, M. Pileni, Langmuir 13 (1997) 3927–3933.
[18] A. Gupta, M. Gupta, Biomaterials 26 (2005) 1565–1573.
[19] A. Gupta, M. Gupta, Biomaterials 26 (2005) 3995–4021.
[20] U. Jeong, X. Teng, Y. Wang, H. Yang, Y. Xia, Adv. Mater. 19 (2007) 33–60.
[21] F. Jiang, C. Wang, Y. Fu, R. Liu, J. Alloys Compd. 503 (2010) L31–L33.
[22] X. Teng, H. Yang, J. Mater. Chem. 14 (2004) 774–779.
[23] J. Lee, T. Isobe, M. Senna, J. Colloid Interface Sci. 177 (1996) 490–494.